Math Geosci (2016) 48:439–461
DOI 10.1007/s11004-015-9619-5

On the Initial Stages of the Densification and Lithification of Sediments

C. M. Sands[1] · **H. W. Chandler**[1]

Received: 12 March 2015 / Accepted: 1 September 2015 / Published online: 24 September 2015

Abstract This paper presents a model that can simulate early rock-forming processes, including the influence of the initial packing of the grains on the subsequent rearrangement that occurs as a consequence of pressure-induced grain damage. The paper is concerned with the behaviour of assemblies of loose grains and the mechanics of early lithification. Consider the concept of shear-induced negative dilatancy, where any shear deformation has a tendency to produce densification even at very low pressures. As shear deformation progresses, positive dilatancy starts to contribute and at the critical state the two effects balance. This concept is encapsulated within the mathematics of the model. The model building scheme is first outlined and demonstrated using a hard particle model. Then, the concept of 'self cancelling shear deformations' that contribute to the shear–volume coupling but not to the macroscopic shear deformation is explained. The structure of the hard particle model is modified to include low levels of damage at the grain contacts. A parameter that describes bonding between the grains and possible damage to those bonds is incorporated into a term that, depending on its magnitude, also accounts for frictional resistance between unbonded grains. This parameter has the potential to develop with time, increasing compressive stress, or in response to evolving chemical concentrations. Together these modifications allow densification in the short term, and the formation of sedimentary rocks in the long term, by pressure alone, to be simulated. Finally, simulations using the model are compared with experimental results on soils.

Keywords Constitutive modelling · Critical state · Yield surface · Rock forming · Consolidation · Lithification

✉ C. M. Sands
c.sands@abdn.ac.uk

[1] University of Aberdeen, Aberdeen AB24 3UE, UK

1 Introduction

When rock surfaces grind together during earthquakes or fault movement (Mair and Abe 2008; Wibberly et al. 2008), fine particles become detached from the rock surface. The particles are subsequently ground to finer material and, depending on the mineral content of the parent rock, sands, silts and clays are formed. Non-mechanical processes, such as freeze–thaw and repeated heating and cooling, also contribute to the production of granular assemblies. Slow consolidation increases the density of clay sediments such that slates and shales eventually form (Baker et al. 1993; Ellis and Darby 2005).

The rearrangement of un-bonded granular materials (Paterson and Tobisch 1993) subjected to shear and moderate compression is important in many geomechanical situations. Shear, particularly cyclic shear, facilitates the rearrangement of loose sand grains into a denser packing, particularly when supported by moderate pressure or liquefaction during earthquakes (Gratchev et al. 2006; Dan et al. 2009). The deposition of cementing minerals and crystal growth at the inter-granular contacts then results in the formation of sandstones.

Slope instability (Cashman and Cashman 2000) is exacerbated by shear stresses, such as those that occur during earthquakes or are generated by human activity. Slip of sub-sea slopes can result in tidal waves. Shear stresses caused by vibrating equipment or the transport of fluids can result in other difficulties, such as sand production from oil reservoirs (Han and Dusseault 2005). It follows that a better understanding of the mechanisms that produce shear stresses and pressure in granular assemblies (both bonded and unbonded) together with an improved ability to predict the material response to those stresses is of obvious importance.

While it is common to lump the above mechanisms together and assume an elastic (Fokker and Orlic 2006) or viscoelastic (Hermanrud et al. 2013) material response, the relatively recent acknowledgement of the presence of localised compaction bands (Mollema and Antonellini 1996) in some sandstones, but not in others, has initiated extensive experimental and theoretical investigations (Baud et al. 2006; Holcomb et al. 2007). This concern has also been investigated for carbonate rocks (Cilona et al. 2012; Das and Buscarnera 2014). Experimental investigations of yield surfaces clearly confirm the importance of shear (or differential) stress, in addition to pure pressure, in the compaction process and approximately elliptical yield envelopes are found (Baud et al. 2006). Although the fracture, disaggregation and rearrangement of grains are reported (Holcomb et al. 2007), consideration of their relative contribution does not form part of the constitutive models used to quantify their behaviour. For the model presented in this paper, an attempt is made to identify the roles of these different mechanisms. Specifically, three types of densification are postulated: (1) complete rigid-grain rearrangement during shearing, without any pressure effect, at very low pressures in the absence of negative dilatancy; (2) rigid ‘cooperative’ motion of the grains requiring only very minor damage at the grain to grain contacts that is enhanced by a loose initial packing; (3) grain motions dominated by significant crushing either locally at the contacts or of the whole grain.

The concept that granular assemblies can achieve a denser packing as a result of grain rearrangement caused by shearing is widely accepted (Mair and Abe 2008; Chupin et al. 2011). On the other hand, the possibility that mechanisms might exist

by which granular assemblies could densify by grain rearrangement under the influence of pressure alone has not been extensively investigated as an explicit part of the modelling process. This paper explores that possibility and presents the concept of 'self-cancelling' shear deformation whereby granular rearrangement can occur as a consequence of shear strains at the microscopic level that cancel each other out at the macroscopic level (Sands and Chandler 2012, 2014). Additionally, a parameter is introduced that controls the development of inter-particle bonding. Currently, this parameter depends only on the amount of inter-particle bonding present, but it has the potential to be a function of time, effective pressure, temperature and the chemical composition of the interstitial fluid. At present, this bonding parameter has a single strength value and so can only simulate a brittle bond that looses all its strength once a maximum value of tension is exceeded; or a constant cohesion, or 'liquid bonding' between the particles, that is always present.

First, the mechanisms of compaction and how they can be modelled are explored, and then the model construction is outlined. That modelling procedure is then illustrated by applying it to a simple hard particle model into which self-cancelling shears and bond development are subsequently incorporated. The evolution equations are then presented followed by an examination and explanation of the yield surfaces that the model produces. Finally, some illustrative simulations are presented and the paper closes with some concluding remarks.

2 Background

To better understand the mechanisms of compaction, it may be helpful to start by considering some simple aspects of the process. When sand is poured into a container, the particles immediately rotate and rearrange to increase the packing density. The reduction in gravitational potential drives the frictional dissipation at the particle contacts. The packing quickly becomes more difficult to densify and grain rearrangement stops. If the particles are sufficiently hard, stiff and strong, the application of a monotonically increasing load on the top surface produces little densification beyond that produced under gravity alone. It is well known, however, that one can increase the density of sand in this condition either by applying cyclic shear (Youd 1972) at low effective pressures or by applying effective pressures that produce damage and deformation at the particle–particle contacts (Vesic and Clough 1968). In both cases, further particle rotation and rearrangement are likely to occur. As densification continues, these rotations become less significant and contact deformation starts to dominate.

Historically, continuum models of the behaviour of unbonded granular matter were designed only to account for monotonically increasing deformation. Although a very few treatments proposed that compaction occurred at a critical value of hydrostatic pressure, the vast majority of compaction models included shear enhanced compaction and incorporated either an elliptical yield surface (Roscoe and Burland 1968) or a cone and a cap (DiMaggio and Sandler 1971). These composite surfaces reflect particle crushing on the cap and particle rearrangement on the cone. In some, the model assumptions produce a smooth transition between cap and cone (Chandler 1990), while in others an *ad hoc* smoothing function is inserted (DorMohammadi and Khoei

2008). Some models were modified to cope with kinematic hardening, when the cone swings in response to deformation (Gajo and Muir Wood 1999; Pestana et al. 2002a). Others concentrated on modelling densification by cyclic shearing alone (Youd 1972).

Although generally developed to simulate the behaviour of soils—where intergranular bonding is absent—models of this type have been used to simulate the behaviour of soft rocks (Cuss et al. 2003; Baud et al. 2006). The circumstance that both materials operate in compressive regimes, and the existence in many soil models of a cohesion parameter that captures the influence of interfacial tensions, has enabled such models to be applied to rocks with relative ease. These models can work well but lack an underlying micromechanical rationale needed to facilitate further development or refinement.

Early models of granular plasticity introduced a yield surface and then determined a flow rule, either using the associated flow rule or by introducing a plastic potential function and assuming a flow rule associated to that function. Hunter (1976) suggested that the use of an independent potential function limits the flow rules unnecessarily, and independent flow rules have been used, (Gajo and Muir Wood 1999). Perhaps the most significant disadvantage of using an independent potential function is that it does not allow micromechanical concepts to be properly incorporated into the macroscopic constitutive description. More recently, starting with a dissipation function and dilatancy rule and deducing a yield surface have become popular. This can be done in a number of ways. Ziegler (1983) suggested one scheme and, using the mathematical theory of envelopes, Chandler (1985) obtained the same results. More recently, Chandler and Sands (2007a) updated the envelope approach as an optimisation problem and similar schemes are now used more widely, for example Tsegaye and Benz (2014). Collins and Houlsby (1997) used Legendre transforms in the context of thermodynamics as their rationale, and thermodynamic approaches remain popular (Zhu and Arson 2014).

In this paper, an approach is used that facilitates this incorporation and improves a model, originally developed to simulate the behaviour of saturated sands, to incorporate the effect of pressure in aiding densification and suppressing dilation as well as the introduction of inter-granular bonding.

3 Model Building Scheme

The modelling scheme used in this paper starts by postulating: (1) an energy conserving kinematic rule linking the shear and volumetric strains induced by the rearrangement of essentially rigid grains; and (2) a dissipation function that encapsulates the conversion of work into heat by frictional sliding and/or by grain damage. It is then assumed that only when sufficient work has been done to satisfy the requirements of the dissipation function will deformation occur. This latter condition is found by maximising the dissipation rate (Ziegler 1983) with respect to the strain rate under the principal constraint that the rate of doing work is equal to the dissipation rate. This entirely mathematical process produces a rigid-plastic flow rule and a yield criterion.

An approach is then presented that is suitable for modelling the densification of loose granular assemblies that often occurs during lithification. In the resulting model,

hydrostatic pressure alone can produce compaction with the minimum of particle damage. This outcome is achieved via additional terms in both the established kinematic constraint and the dissipation function that capture the rotational deformation occurring at inter-particle contacts within granular assemblies undergoing deformation.

Specifically, the reader is asked to imagine positive and negative shear strains varying over a small length scale that cancel each other out macroscopically. The overall rate of this complex micro-scale particle rearrangement is represented by a single positive scalar variable, $\dot{\alpha}$. This variable is incorporated within the kinematic constraint and the dissipation function so that the model is able to simulate pressure-enhanced compaction. It is postulated that this mode of deformation is associated with some small scale increase in particle to particle contact area, which is captured within two additional terms in the dissipation function. A bonding parameter incorporates the effect of the increased contact area that occurs as a consequence of bond material growth. Another additional term, that is not associated with particle rearrangement, is included within the dissipation function and accounts for the increase in contact area that occurs as a result of particle damage at the contacts. Both these terms have the potential to evolve with time, temperature, stress, and chemical concentration.

This paper makes use of the convention that tension is positive and works entirely in terms of effective (rather than total) stress. First, consider a loosely packed, unbonded granular assembly of unit volume in a Cartesian coordinate system x_1, x_2 and x_3. It is subjected to components of macroscopic effective stress σ_{ij} and undergoes components of macroscopic strain e_{ij}. In this context, macroscopic means that they are volume averages and that while the assembly is non-uniform locally, it is regarded as homogeneous if the unit volume contains at least 1000 grains. The mean effective stress using the Einstein summation convention is $\sigma = \sigma_{mm}/3$ and, similarly, the volume strain is $e = e_{mm}$. Deviatoric components of stress and strain are defined as

$$s_{ij} = \sigma_{ij} - \sigma\delta_{ij} \tag{1}$$

and

$$d_{ij} = e_{ij} - e\delta_{ij}/3, \tag{2}$$

where δ_{ij} is the Kronecker delta. Note that a list of notation used in this paper is provided in Table 1.

A dot over the relevant symbol indicates a rate, or increment, and so the rate of doing work on the assembly ($\dot{w}$) can then be written as

$$\dot{w} \equiv s_{ij}\dot{d}_{ij} + \sigma\dot{e}\,. \tag{3}$$

If viewed on the local scale, one might expect a contribution from the product of the fluctuations of the components of stress and strain, but this product is zero (Bishop and Hill 1951), as the assembly is macroscopically homogeneous. For the rigid plastic idealisation, an energy balance can then be written as

$$s_{ij}\dot{d}_{ij} + \sigma\dot{e} = \dot{D}(\sigma, \dot{d}_{ij}, \dot{e}), \tag{4}$$

where $\dot{D}$ is the rate of dissipation. This function is always positive, and, to ensure the strain rate independence typical of sands, is homogeneous of degree one in the strain rate components. That is, if each component of the strain rate tensor is doubled, then the rate of dissipation is doubled.

To better illustrate the model building procedure, it is first applied to a three-dimensional version of a two-dimensional, hard particle model developed by the current authors that has been shown to successfully simulate the behaviour of unbonded granular assemblies (Chandler and Sands 2007b). The model is then extended to incorporate various forms of damage at the particle contacts. These modifications allow the model to be used to simulate the behaviour of cemented rock as well as assemblies of unbonded grains. The model can simulate the detachment of intact grains and rotations at a microstructural scale during compaction by pressure alone, and the suppression of dilation at moderate pressures, as well as compaction associated with full grain crushing.

4 Hard Particle Model

The model development procedure is illustrated using a rate-independent model of an unbonded, granular material, where grains are not damaged or deformed—the hard particle model. A sophisticated dilatancy rule presented in earlier work (Chandler and Sands 2007b) is implemented in this model. In that paper, a two-dimensional version of the hard particle model was used successfully to simulate some experimental results (Joer et al. 1998). That work demonstrated the ability of this dilatancy rule to capture all the important features of both monotonic and cyclic deformation even when the principal axes rotate. This dilatancy rule is given by

$$\dot{e} = \nu_i \sqrt{\dot{d}_{mn}\dot{d}_{mn}} + 2\nu_r (d_{ij} - d^r_{ij})\dot{d}_{ij}, \tag{5}$$

where ν_i and ν_r are coefficients of isotropic and rotational dilation, respectively, and are functions of the current density and d^r_{ij} is defined by the differential equation

$$\dot{d}^r_{ij} = c_1 (d_{ij} - d^r_{ij}) \sqrt{\dot{d}_{mn}\dot{d}_{mn}}, \tag{6}$$

where c_1 is a measure of how quickly the material reaches the critical state if the grains are rigid, and is assumed to be constant. As the hard particle model is unbonded and can only operate within a compressive regime ν_i is negative, permitting compaction to be simulated, while ν_r is positive, and both are dependent on the current volume (Chandler and Sands 2007b). As ν_i and ν_r have different signs, they oppose each other, permitting the development of the critical state when they cancel each other out, and the dramatic increase in density on strain-rate reversal observed by others (Yunus et al. 2010). ν_r controls the rotational aspect of the kinematic hardening, producing the non-coaxiality of stress and strain rate observed experimentally (Joer et al. 1998).

It has been shown (Chandler and Sands 2007b) that the dilatancy rule presented in Eq. 5 will correctly predict: the non-coaxiality of the stress and strain rate, critical

state behaviour, and cyclic densification. As there is no characteristic material stress (for example, a particle strength or a specified preconsolidation pressure), the model cannot simulate the suppression of dilatancy by high pressure, but that capability is developed for the present model in Sect. 5. The isotropic dissipation rate is defined as

$$\dot{D} \equiv -\mu\sigma\sqrt{\dot{d}_{mn}\dot{d}_{mn}}, \tag{7}$$

where μ is an effective friction coefficient.

The next step in the modelling procedure is to produce flow rules and a yield surface and a number of ways exist for producing them (Chandler and Sands 2010). In this model the principle of maximum dissipation rate is applied under the explicit constraint that all the work done is dissipated. An additional constraint that the dissipation rate is finite is also included. For completeness, the requirement that $\dot{d}_{mm} = 0$ is explicitly enforced, although in this case the dissipation function and dilatancy rule are such that the Langrangian multiplier is zero (Chandler and Sands 2007a). Equation 5 is also directly incorporated into the rate of doing work ($\dot{w}$).

An appropriate Lagrangian function, incorporating Lagrangian multipliers (ϕ, ϖ and κ), is

$$L = \dot{D} - \phi(\dot{w} - \dot{D}) - \varpi(\dot{D}_0 - \dot{D}) - \kappa\dot{d}_{mm}, \tag{8}$$

where $\dot{D}_0$, the nominal rate of dissipation, is a positive constant that is required to produce a unique solution to the optimisation problem. The term

$$\tilde{s}_{ij} \equiv s_{ij} + 2\nu_r(d_{ij} - d^r_{ij})\sigma, \tag{9}$$

is defined and used with Eq. 3, to substitute for $\dot{w}$ in the Lagrangian, which is then differentiated to find an optimality condition

$$\frac{\partial L}{\partial \dot{d}_{ij}} = -\phi\left(\tilde{s}_{ij} + \sigma\nu_i\frac{\dot{d}_{ij}}{\sqrt{\dot{d}_{mn}\dot{d}_{mn}}}\right) + (1+\phi+\varpi)(-\mu\sigma)\frac{\dot{d}_{ij}}{\sqrt{\dot{d}_{mn}\dot{d}_{mn}}} - \kappa\delta_{ij} = 0. \tag{10}$$

A contraction with δ_{ij} determines that $\kappa = 0$ and, using that result, Eq. 10 can be rearranged to give the flow rule

$$\dot{d}_{ij} = \frac{\phi\tilde{s}_{ij}\sqrt{\dot{d}_{mn}\dot{d}_{mn}}}{(1+\phi+\varpi)(-\mu\sigma) - \phi\sigma\nu_i}. \tag{11}$$

Equation 10 is then contracted with $\dot{d}_{ij}$ to give

$$-\phi\left(\tilde{s}_{ij}\dot{d}_{ij} + \sigma\nu_i\sqrt{\dot{d}_{mn}\dot{d}_{mn}}\right) + (1+\phi+\varpi)(-\mu\sigma)\sqrt{\dot{d}_{mn}\dot{d}_{mn}} = 0. \tag{12}$$

When $\phi \neq 0$, the equality of the rate of doing work and the rate of dissipation requires that $\varpi = -1$. Equation 11 is then used, with $\varpi = -1$, to eliminate $\dot{d}_{ij}$ from Eq. 12 to produce

$$-\left(\frac{\phi\tilde{s_{ij}}\tilde{s_{ij}}\sqrt{\dot{d}_{mn}\dot{d}_{mn}}}{-\mu\sigma-\sigma\nu_i}+\phi\sigma\nu_i\sqrt{\dot{d}_{mn}\dot{d}_{mn}}\right)+\phi(-\mu\sigma)\sqrt{\dot{d}_{mn}\dot{d}_{mn}}=0; \tag{13}$$

and dividing through by non-zero $\phi\sqrt{\dot{d}_{mn}\dot{d}_{mn}}$ gives the yield criterion

$$\tilde{s_{ij}}\tilde{s_{ij}}=(\mu\sigma+\sigma\nu_i)^2. \tag{14}$$

Taking the negative root of the term in brackets in the above equation produces the yield criterion in the standard form

$$0=\frac{\sqrt{\tilde{s}_{nm}\tilde{s}_{nm}}+\sigma\nu_i}{-\mu\sigma}-1 \tag{15}$$

for all non-zero values of ϕ. This includes kinematic hardening as a consequence of the dilatancy rule. Like the original Drucker–Prager yield criterion, this yield criterion is a cone in principal effective stress space.

5 Incorporation of Self-cancelling Shears and Dond Development

5.1 What are 'Self-Cancelling Shears'?

It is well recognised that the volume of a granular assembly can alter if it is subjected to shear. This is usually attributed, mainly, to a rearrangement of the granules into a different packing. Under such a deformation regime, the granules can be regarded as sensibly rigid. Volume change resulting from changes in pressure is usually attributed to elastic or plastic deformation of the granules in an essentially unaltered packing arrangement. The mechanism referred to as 'self cancelling shears' is envisaged as one that can cause volume change in a granular assembly by pressure-induced granule rearrangement. It is postulated that shears at a microscopic level cause very local very minor damage that facilitates localised granule rearrangement into a denser packing. It is further postulated that those shears (at the local, microscopic, level) balance out so that there is no shear at the macroscopic level. It can be seen from the schematic shown in Fig. 1 that this is kinematically possible. Locally, small blocks of material are experiencing shear (the blocks are changing shape) as well as a reduction in size. The shape of the assembly, however, has not changed (it remains square throughout) but the area has reduced. Figures 2 and 3 illustrate the physical changes that, it is postulated, occur at the microscopic level of the inter-granular contacts where minor damage and shear stresses local to the granule contacts facilitate in granule rearrangement resulting in increased density. Figure 2 shows the granule arrangement before the application of pressure produces minor damage local to the inter-granular contacts permitting the rearrangement and densification shown in Fig. 3.

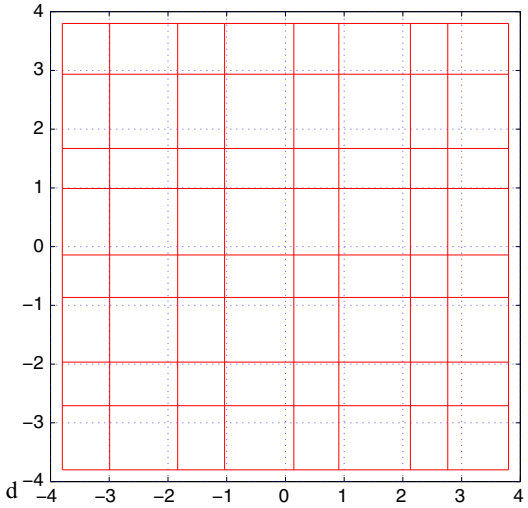

Fig. 1 Schematic illustrating a notional body prior to application of pressure (*dotted blue lines*) and after localised shear has resulted in reduced size (*solid red lines*) while retaining the *original square shape*

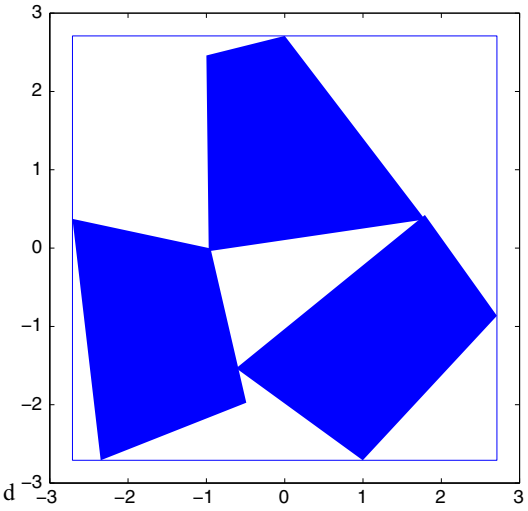

Fig. 2 Schematic illustrating particles prior to application of pressure

5.2 Incorporation into the model

Firstly, in recognising that the particles are vulnerable to damage, the strains are further split into those parts of the volumetric and deviatoric strain rates that are associated only with grain rearrangement ($\dot{e}^R$ and $\dot{d}^R$) and those that are associated only with grain damage ($\dot{e}^D$). As a consequence, the work done becomes

$$\dot{w} = s_{ij}\dot{d}^R_{ij} + \sigma\dot{e}^R + \sigma\dot{e}^D. \tag{16}$$

Implicitly, the local deformation associated with $\dot{e}^D$ is taken to be affine, keeping the angular relationships of the particles constant. Secondly, in addition to the macro-

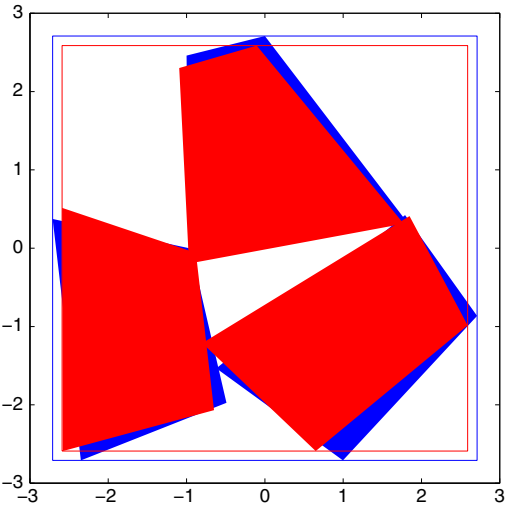

Fig. 3 Schematic illustrating particles after the application of pressure (shown *red*) overlying their original position (shown in *blue*). Minor damage local to the contacts caused by the pressure has permitted granules to rearrange

scopic deviatoric strains (d_{ij}^R), it is postulated that shear strains at particle level might contribute to the dilatancy and to the dissipation rate, but cancel each other out to produce no net macroscopic shears. These include particle rotation as well as damage. The rate of these self-cancelling shears is denoted by the scalar $\dot{\alpha}$. The dilatancy rule is then modified to give

$$\dot{e}^R = v_i \sqrt{\dot{d}_{mn}^R \dot{d}_{mn}^R + \dot{\alpha}^2} + 2v_r (d_{ij}^R - d_{ij}^r)\dot{d}_{ij}^R. \tag{17}$$

In the hard particle model presented in Sect. 4, v_i was negative. This is still the case for compressive regimes and provides the driving force for rearrangement under pure compression.

The extra dissipation rates are incorporated into the dissipation function to give

$$\dot{D} \equiv \sqrt{(c - \mu\sigma)^2 \dot{d}_{mn}^R \dot{d}_{mn}^R + (\dot{e}^D)^2 l^2 + k^2 \dot{\alpha}^2} \tag{18}$$

where c, l and k are measures of the resistance at the particle to particle contacts associated with sliding, crushing and rotation and, hence, have units of stress. To better understand how they function, it is helpful to consider an assembly of solid grains that is in the densest packing arrangement that can be achieved by rearrangement alone. Further densification can only occur as a consequence of significant crushing or squashing at the particle contacts or by particle disintegration. Further densification of this type is controlled entirely by the parameter l. If, however, the particles were not in their densest packing arrangement, further densification by rearrangement would be facilitated by damage at the particle contacts, even if that damage were very small. This process is controlled by the parameter k.

The resistance to sliding is controlled by c and μ. It follows that c, l and k are all influenced by bond development, but only c is solely dependent on the increasing

bond strength that arises as more bonding material is deposited, or the strength of the bonding material itself develops. If the bond breaks, c can be set to zero such that the resistance to sliding at the particle to particle contact depends only on the friction parameter, μ. l reflects the increase in particle to particle contact area, which comes from a combination of particle contact crushing and increase in the area of the bonding material at the particle to particle contacts. It also includes any increase in the number of contacts.

As the contact area (and l) increases, the load that can be supported at the contact also increases, which is true even in the absence of bond material. The ability of the particle to particle contacts to resist rotation is influenced by the area of the contacts, as the larger the contact area, the more they are able to resist rotation. Bond material influences such resistance, but some resistance remains even in an unbonded assembly.

At first sight, it might appear that compaction by hydrostatic pressure alone could be captured by the parameter l. Any attempt to do so, however, would produce a vertex in the yield surface when $\tilde{s}_{ij}\tilde{s}_{ij} = 0$. The incorporation of self cancelling shears removes this vertex. As the self-cancelling shears cancel out macroscopically, they induce no additional work through $s_{ij}\dot{d}^R_{ij}$, but only via $\sigma\dot{e}^R$ as they contribute only to the volume strain rate. This behaviour relies on the result (Bishop and Hill 1951) that the work done can be determined by knowing only the volume averages of the components of stress and strain. The same process as was used in Sect. 4, and the short-hand defined in Eq. 9, is then used to write the Lagrangian concisely as

$$L = \dot{D} - \phi(\dot{w} - \dot{D}) - \varpi(\dot{D}_0 - \dot{D}) - \kappa\dot{d}^R_{mm} \tag{19}$$

and more expansively as

$$\begin{aligned} L = {} & (1 + \phi + \varpi)\sqrt{(c - \mu\sigma)^2\dot{d}^R\dot{d}^R + l^2(\dot{e}^D)^2 + k^2\dot{\alpha}^2} \\ & -\phi\left(\tilde{s}\dot{d}^R_{ij} + \dot{e}^D\sigma + \sigma\nu_i\sqrt{\dot{d}^R_{ij}\dot{d}^R_{ij} + \dot{\alpha}^2}\right) - \kappa\dot{d}^R_{mm}; \end{aligned} \tag{20}$$

while its partial derivatives are

$$\frac{\partial L}{\partial \dot{d}^R_{ij}} = (1 + \phi + \varpi)\frac{(c - \mu\sigma)^2\dot{d}^R_{ij}}{\dot{D}} - \phi\left(\tilde{s}_{ij} + \frac{\sigma\nu_i\dot{d}^R_{ij}}{\sqrt{\dot{d}^R_{ij}\dot{d}^R_{ij} + \dot{\alpha}^2}}\right) - \kappa\delta_{mm} = 0, \tag{21}$$

$$\frac{\partial L}{\partial \dot{e}^D} = (1 + \phi + \varpi)\frac{l^2\dot{e}^D}{\dot{D}} - \phi\sigma = 0, \tag{22}$$

and

$$\frac{\partial L}{\partial \dot{\alpha}} = (1 + \phi + \varpi)\frac{k^2\dot{\alpha}}{\dot{D}} - \phi\left(\frac{\sigma\nu_i\dot{\alpha}}{\sqrt{\dot{d}^R_{ij}\dot{d}^R_{ij} + \dot{\alpha}^2}}\right) = 0. \tag{23}$$

On contracting Eq. 21 with δ_{ij}, it is immediately apparent that again $\kappa = 0$. Multiplying Eq. 21 by $\dot{d}^R_{ij}$, Eq. 22 by $\dot{e}^D$ and Eq. 23 by $\dot{\alpha}$ and adding the results gives $L = 0$; and so again $\varpi = -1$, as all the work done is being dissipated, and ϕ can take any non-zero value.

For $\dot{\alpha} \neq 0$, Eqs. 21–23 reduce to

$$\dot{d}^R_{ij} = \dot{D}\frac{\tilde{s}_{ij}}{(c-\mu\sigma)^2 - k^2}, \tag{24}$$

$$\dot{e}^D = D\frac{\sigma}{l^2}, \tag{25}$$

and

$$\sqrt{\dot{d}^R_{ij}\dot{d}^R_{ij} + \dot{\alpha}^2} = \dot{D}\frac{\sigma v_i}{k^2}. \tag{26}$$

Note that Eq. 26 has been used in obtaining Eq. 24. Substituting the above into the Lagrangian gives

$$\frac{\tilde{s}_{ij}\tilde{s}_{ij}\dot{D}}{(c-\mu\sigma)^2 - k^2} + \dot{D}\frac{\sigma^2 v_i^2}{k^2} + \dot{D}\frac{\sigma^2}{l^2} - \dot{D} = 0, \tag{27}$$

leading to

$$0 = \sqrt{\frac{\tilde{s}_{ij}\tilde{s}_{ij}}{(c-\mu\sigma)^2 - k^2} + \frac{\sigma^2 v_i^2}{k^2} + \frac{\sigma^2}{l^2}} - 1, \tag{28}$$

for $\dot{D} \neq 0$. Eq. 28 is a yield surface and forms a smooth cap (see Fig. 4). Note that, when $\tilde{s}_{ij}\tilde{s}_{ij} = 0$

$$\sigma^2 = \frac{k^2 l^2}{v_i^2 l^2 + k^2}, \tag{29}$$

allowing the definition

$$p^* = \sqrt{\frac{k^2 l^2}{v_i^2 l^2 + k^2}}, \tag{30}$$

where p^* is the highest pressure on the yield surface.

For the case where $\dot{\alpha} = 0$, Eqs. 21 and 22 become

$$\dot{d}^R_{ij} = \frac{\dot{D}\tilde{s}_{ij}}{(c-\mu\sigma)^2 - \sigma v_i \dot{D}/\sqrt{\dot{d}^R_{mn}\dot{d}^R_{mn}}}, \tag{31}$$

and

$$\dot{e}^D = D\frac{\sigma}{l^2}. \tag{32}$$

The first of these, when contracted with itself, yields

$$\sqrt{\dot{d}^R_{mn}\dot{d}^R_{mn}} = \dot{D}\frac{\sqrt{\tilde{s}_{ij}\tilde{s}_{ij}} + \sigma v_i}{(c-\mu\sigma)^2}, \tag{33}$$

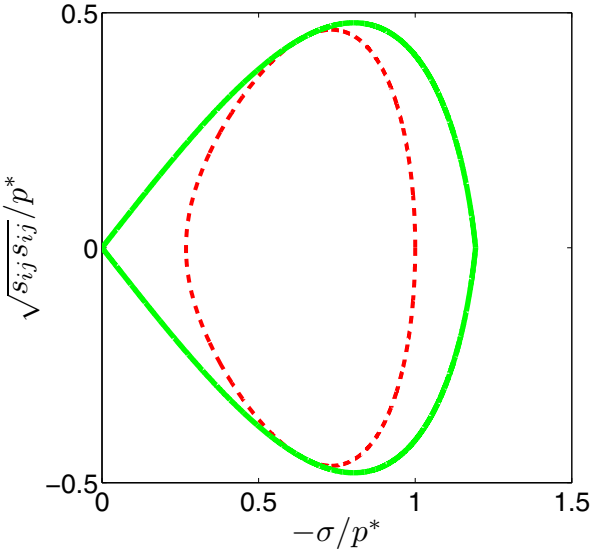

Fig. 4 Sections in the $(-\sigma/p^*)$, $(\sqrt{s_{ij}s_{ij}}/p^*)$ plane through two yield surfaces: a cone at low pressure and a cap at higher pressure, with no inter-particle bonding. The *solid line* shows the yield surface presented in Eq. 35 while the *broken line* shows that presented in Eq. 28. (See Table 2, for parameter values: $c = 0$, $v_r = 0$; $d^g_{ij} = 0$.)

which, upon substitution, reduces Eq. 31 to

$$\dot{d}^R_{ij} = \tilde{s}_{ij}\dot{D}\frac{\sqrt{\tilde{s}_{ij}\tilde{s}_{ij}} + \sigma v_i}{\sqrt{\tilde{s}_{ij}\tilde{s}_{ij}}(c - \mu\sigma)^2}. \tag{34}$$

Elimination of $\dot{d}^R_{ij}$ and $\dot{e}^D$ in the energy balance ($\dot{w} = \dot{D}$) gives, for $\dot{D} \neq 0$, the yield criterion

$$0 = \sqrt{\frac{(\sqrt{\tilde{s}_{ij}\tilde{s}_{ij}} + \sigma v_i)^2}{(c - \mu\sigma)^2} + \frac{\sigma^2}{l^2}} - 1. \tag{35}$$

As shown in Fig. 4, this relationship forms a curved cone (the solid green line) and meets smoothly with the cap (the red dashed line) when $\dot{\alpha} = 0$. If the cap (when $\dot{\alpha} \neq 0$) was not used, but the cone was permitted to continue, it would form a vertex where $\sqrt{\tilde{s}_{ij}\tilde{s}_{ij}} = 0$, as can be seen in the figure. Avoiding prediction of this non-physical behaviour is one of the principal justifications for the development of self-cancelling shears.

When the mean stress is tensile (negative pressure), then the previous tendency to compact on shear, when subject to positive pressure, changes to a tendency to dilate. This state is reflected in the model as a switch to a positive value of v_i. In the yield surfaces presented here, this is simply the negative of the value of v_i used in the compressive regime, although other values might be used if appropriate. The change

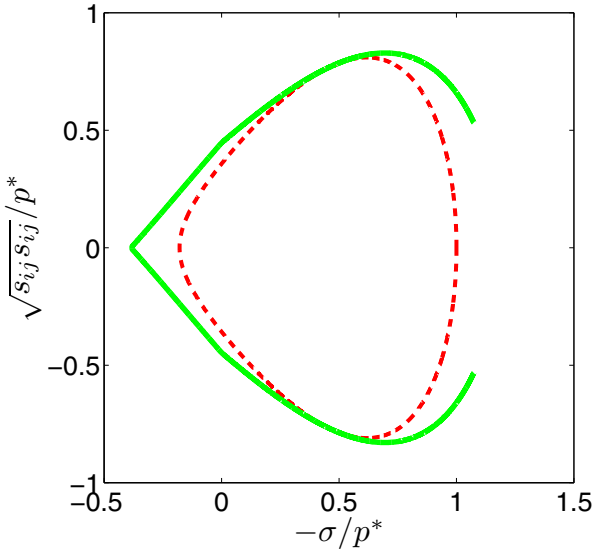

Fig. 5 Sections in the $(-\sigma/p^*)$, $(\sqrt{s_{ij}s_{ij}}/p^*)$ plane through two yield surfaces: a cone at low pressure and a cap at higher pressure, with inter-particle bonding. The *solid line* shows the yield surface presented in Eq. 35 while the *broken line* shows that presented in Eq. 28. (See Table 2 for parameter values: $c = 0.5$; $\nu_r = 0$; $d_{ij}^g = 0$.)

in the value of ν_i produces a kink in the yield surface when $\sigma = 0$, as can be seen in Fig. 5.

6 Evolution Equations

The parameter l, which is positive, is assumed to evolve in accordance with

$$l = l_0 \left(\exp\left(\frac{(V_\mathrm{R} - V)}{\lambda} \right) - 1 \right) \tag{36}$$

where l_0 is a measure of the grain strength, V is the current specific volume of the granular assembly (bonded or unbonded) and V_R is a reference-specific volume. This reference volume is the volume that the assembly would occupy if it were in an imaginary state in which all the particles retained their current relative positions and orientations, but were returned to their initial, undamaged, shape. It follows that, if $V_\mathrm{R} - V$ is very small, very little squashing or crushing has occurred at the particle contacts. λ is a material constant such that $l_0\lambda$ contributes to the stiffness of the granular assembly.

For each increment of load, V and V_R are updated using

$$V = V(1 + \dot{e}) \tag{37}$$

and

$$V_{\mathrm{R}} = V_{\mathrm{R}}(1 + \dot{e}^{R}). \tag{38}$$

The parameter k is maintained at a constant multiple of l, while the evolution of ν_i and ν_r is governed by

$$\nu_i = -c_2 \left(\frac{V_{\mathrm{R}} - V_{\mathrm{D}}}{V_{\mathrm{D}}} \right) \tag{39}$$

and

$$\nu_r = c_3 \left(\frac{V_{\mathrm{L}} - V_{\mathrm{R}}}{V_{\mathrm{D}}} \right) \tag{40}$$

where c_2 and c_3 are material constants that can be determined from shear tests (c_1 controls the shear strain, and c_2 the density, at the critical state) and V_{D} and V_{L} are the densest and loosest specific volumes that the assembly can achieve at low pressure. Guidance on how to determine, from geotechnical tests, the values of most of the parameters used for the models presented in this paper can be found in other work by the authors (Sands and Chandler 2011).

7 Discussion of Yield Surfaces

Let us investigate some properties of the two yield functions developed in Sects. 4 and 5. To better understand Eq. 35 and how it combines with Eq. 15, it may be helpful to consider Figs. 4, 5, 6, 7, 8 and 9. If $\nu_r = 0$, the yield surface has an axis of symmetry about the hydrostatic axis, as shown in Figs. 4, 5 and 6. When $\nu_r \neq 0$, the model will predict kinematic hardening and a distorted yield surface. When the principal axes of the effective stress tensor and the tensor with components $(d^R_{ij} - d^r_{ij})$ coincide, then this distorted yield surface can be plotted in principal stress space as shown in Fig. 7. It should be noted that the section cut through this yield surface by a constant pressure plane is still circular. In the even more restrictive case of proportional loading from an isotropic state, where $s_{ij} \propto (d^R_{ij} - d^r_{ij})$, the yield surface can be plotted on the $(-\sigma/p^*)$, $(\sqrt{s_{ij}s_{ij}}/p^*)$ plane as shown in Fig. 9.

If the value of c is set to zero, the model mimics an unbonded granular assembly. Figure 4 shows a section through the composite yield surface for such an unbonded granular assembly using the parameters shown in Table 2. It can be noted that the yield surface is in two parts, which merge seamlessly together so that, apart from at the origin, vertices are absent and there is continuity of the first derivative though not of the second derivative. Figure 5 shows a similar section for a bonded granular assembly, with all other material parameters unchanged. Figure 6 shows the yield surface for the bonded granular assembly, decorated with flow vectors indicating the immediate direction of any plastic flow in principal stress space for the material parameters shown in Table 1. Figure 7 shows the yield surface for the bonded granular assembly after kinematic hardening has developed. It is decorated with flow vectors indicating the immediate direction of any plastic flow in principal strain space. The material parameters are shown in Table 1 (note that $d^g_{ij} = d^R_{ij} - d^r_{ij}$).

In addition, it should be noted that c, k and l are the only material parameters with the dimensions of stress, and it should be recalled that l is kept proportional to k. So,

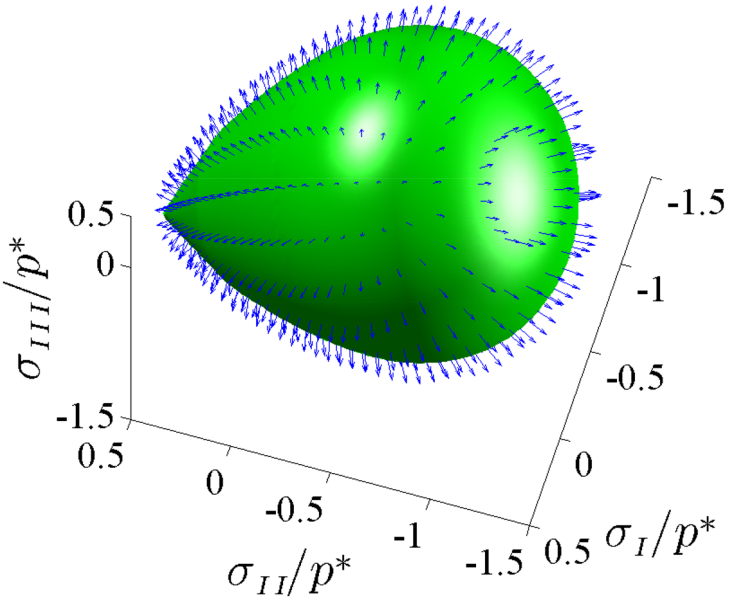

Fig. 6 Yield surface in dimensionless principal stress space decorated with flow vectors for a bonded granular assembly. View not down the hydrostatic axis. (See Table 2 for parameter values: $c = 0.5$; $\nu_r = 0$; $d^g_{ij} = 0$.)

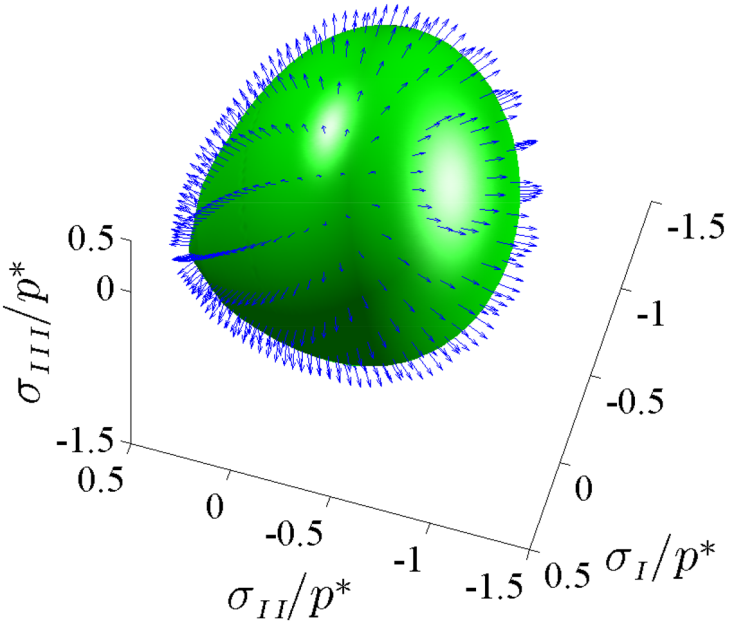

Fig. 7 Yield surface in dimensionless principal stress space decorated with flow vectors for a bonded granular assembly after kinematic hardening. View not down the hydrostatic axis. (See Table 2 for parameter values: $c = 0.5$; $\nu_r = 0.25$; $d^g_{ij} \neq 0$.)

Table 1 Notation

Symbol	Definition
σ_{ij}	Component of the macroscopic effective stress tensor
e_{ij}	Component of the macroscopic strain tensor
s_{ij}	Component of the deviatoric stress tensor
d_{ij}	Component of the deviatoric strain tenor
σ	Mean effective stress
$\dot{e}^R$	Volumetric strain rate (or increment) associated with grain rearrangement
$\dot{e}^D$	Volumetric strain rate (or increment) associated with grain damage
d_{ij}^R	Component of the deviatoric strain tensor associated with grain rearrangement
$\dot{d}_{ij}$	Component of the deviatoric strain rate (or increment) tensor
$\dot{\delta}$	Kronecker delta
$\dot{w}$	Rate of doing work
$\dot{D}$	Rate of dissipation
$\dot{D}_0$	Nominal rate of dissipation
ν_i	Coefficient of isotropic dilatancy
ν_r	Coefficient of rotational kinematic dilatancy
$\dot{\alpha}$	Rate (or increment) of 'self cancelling shears'
L	Lagrangian
ϕ, ϖ, κ	Lagrangian multipliers
μ	Friction coefficient
l	Parameter controlling densification by grain damage
k	Parameter controlling densification by grain rearrangement
c	Bond strength parameter

Guidance on how to determine, from geotechnical tests, the values of most of the parameters used for the models presented in this paper can be found in other work by the authors (Sands and Chandler 2011)

if μ, ν_i and ν_r are held constant and c is also proportional to k, the size of the yield function shown in Fig. 7 scales with k. This model is intended to simulate the behaviour of granular materials with relatively small specific volumes, so the sum $\nu_i + \mu$ is kept positive, preventing the collapse of unbonded assemblies that can otherwise occur at low positive pressures.

If $\sqrt{\tilde{s}_{ij}\tilde{s}_{ij}} = 0$, then the model including self-cancelling shears predicts compaction with no shape change. For the case where $\nu_r = 0$, the model predicts that this occurs under hydrostatic compression. To cope with the full range of pressure from zero to p^* (defined in Eq. 30), the yield surface produced by Eq. 28 must be augmented by the yield surface where $\dot{\alpha} = 0$ given by Eq. 35. When $\nu_r \neq 0$ and $d_{ij}^g \neq 0$, the cone swings about the origin, as can be seen from Figs. 7 and 9. However, the cone merges smoothly with the cap (as can be seen from Fig. 4) and continuity of the yield surface and its first derivative are maintained. Note that an applied hydrostatic stress no longer simply produces a smaller yield surface, instead a change in the shape of the yield surface is predicted.

Table 2 Material parameters

Parameters	Value
μ	1.0
ν_i	0.15
ν_r	$0.0^*/0.25^+$
c	$0.0^*/0.5^+$
k	0.3
l	1.35
d^g_{11}	1.0^+
d^g_{22}	-0.5^+
d^g_{33}	-0.5^+

* No kinematic hardening,
+ with kinematic hardening

Figures 8 and 9 are projections onto the plane of $(-\sigma/p^*)$, $(\sqrt{s_{ij}s_{ij}}/p^*)$. The precise nature of this projection requires some further explanation, particularly with respect to Fig. 9. Recall that

$$\tilde{s}_{ij} \equiv s_{ij} + 2\nu_r(d^R_{ij} - d^r_{ij})\sigma. \tag{41}$$

An appropriate section to take in stress space is one in which

$$s_{ij} = \lambda(d^R_{ij} - d^r_{ij}). \tag{42}$$

This section through the yield surface can then be written using the shorthand $d^g_{ij} \equiv d_{ij} - d^r_{ij}$ as

$$0 = \sqrt{\frac{\left(\sqrt{s_{ij}s_{ij}} + 2\nu_r\sigma\sqrt{d^g_{ij}d^g_{ij}}\right)^2}{(c-\mu\sigma)^2 - k^2} + \frac{\sigma^2}{l^2} + \frac{\sigma^2\nu_i^2}{k^2}} - 1. \tag{43}$$

for the case when $\dot{\alpha} = 0$ and, simultaneously, $\dot{\alpha} \neq 0$.

8 Simulation of Pressure Induced Compaction

Figure 10 shows the results (redrawn) of experiments in isostatic compression by Miura (1979) and Miura et al. (1984) on Toyoura sand, reproduced by Pestana et al. (2002b). The results of experiments on initially loose, medium dense and dense packing are shown as diamonds, squares and circles, respectively. Simulations of those experiments, produced using the model presented here with the parameter values given in Table 3, are shown as chain, solid and dotted lines, respectively. This shows the capacity of the model to simulate isostatic compaction at moderate to high pressures taking the initial packing of the sand grains into account.

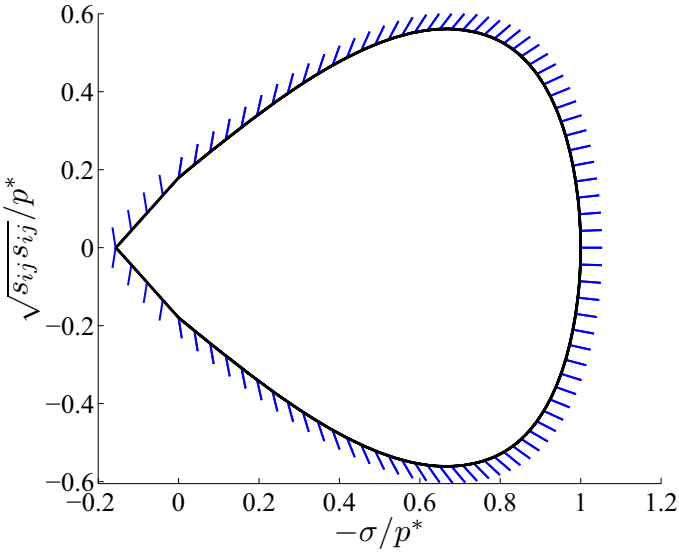

Fig. 8 Sections in the $(-\sigma/p^*)$, $(\sqrt{s_{ij}s_{ij}}/p^*)$ plane through yield surface (including inter-particle bonding) decorated with flow vectors. (See Table 2 for parameter values: $c = 0.5$; $\nu_r = 0$; $d^g_{ij} = 0$.)

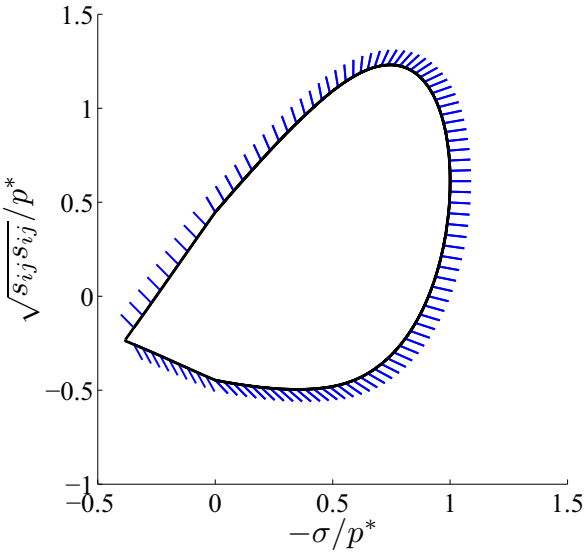

Fig. 9 Sections in the $(-\sigma/p^*)$, $(\sqrt{s_{ij}s_{ij}}/p^*)$ plane through yield surface (including inter-particle bonding and kinematic hardening) decorated with flow vectors. (See Table 2 for parameter values: $c = 0.5$; $\nu_r = 0.25$; $d^g_{ij} \neq 0$)

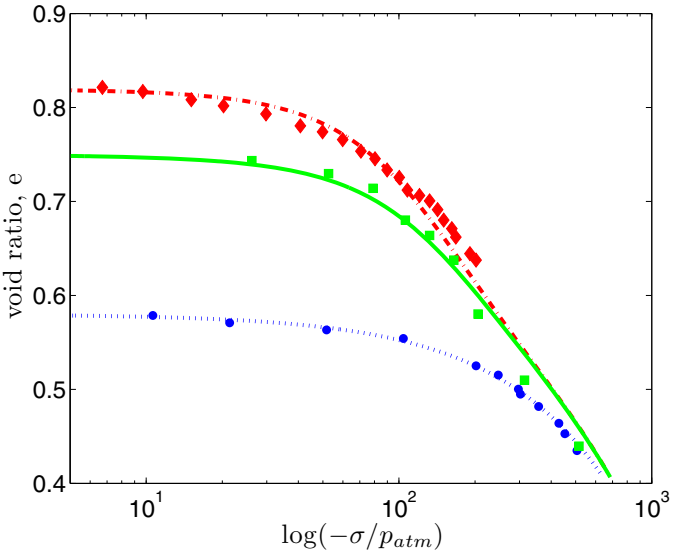

Fig. 10 Simulations (*lines*) of experiments carried out by Miura (1979) and Miura et al. (1984) [and represented by Pestana et al. (2002b)] on soils with different initial packing densities (*diamonds* loose, *squares* medium dense and *circles* dense—redrawn). See Table 3 for parameter values

Table 3 Parameters for Fig. 10

Parameter	Value
μ	1.0
c_1	8.5
c_2	1.3
c_3	30.6
l/k	1.7
l_0	1.45 GPa
V_{L}	1.995
V_{D}	1.58
V (initial)	1.82/1.75/1.58
V_R (initial)	1.82/1.75/1.58
λ	4.0

9 Conclusions

This paper successfully extends an existing hard particle model by introducing particle bonding in addition to particle damage. A feature of the hard particle model is that there are two contributions to the rate of volume change: (1) a continuing densification with shear deformation; and (2) a developing tendency to dilate. These two cancel each other

out at the critical state when the volume remains constant, but on reversal of straining they reinforce each other to produce the dramatic densification seen in experiments.

The model presented here keeps these essential concepts intact but includes particle damage and particle bonding. Particle damage is introduced in two forms: (1) an affine compaction such that the angular relationships of the particles remains constant, and (2) a non-affine contribution that permits those relationships to alter and, hence, incorporates the densification tendency developed in the hard particle model. Particle bonding is introduced via a modification to the frictional term in the dissipation function.

The combination of damage mechanisms used in the model presented here produces a smooth cap that merges perfectly with the curved cone and avoids a vertex in the cap. The model is successfully tested on experimental data from pressure-induced compaction of sands of different initial densities.

In work presented elsewhere (Chandler and Sands 2007a, b; Sands and Chandler 2010, 2014; Sands et al. 2010, 2011), the authors have developed evolution equations for v_i and v_r. Further work is planned to develop evolution equations for c and k (the ratio of k/l will continue to be kept constant). Similarly, a relatively simple dissipation function that predicts a circular cone (akin to the Drucker–Prager model) has been presented here. The authors have shown elsewhere (Chandler and Sands 2009) how a different dissipation function would predict a cone with the traditional Mohr–Coulomb shape and others will predict the Matsuoka-Nakai or Lade-Duncan yield surfaces.

References

Baker DW, Chawla KS, Krizek R (1993) Compaction fabrics of pelites: experimental consolidation of kaonlinite and implications for analysis of strain in slate. J Struct Geol 15(9/10):1123–1137

Baud P, Vajdova V, Wong T (2006) Shear enhanced compaction and strain localization: inelastic deformation and constitutive modeling of four porous sandstones. J Geophys Res Solid Earth 111(B12401) 1–7. doi:10.1029/2005JB004101

Bishop JFW, Hill R (1951) A theory of the plastic distortion of a polycrystalline aggregate under combined streses. Philos Mag 42(327):414–427

Cashman S, Cashman K (2000) Cataclaisis and deformation-band formation in unconsolidated marine terrace sand, Humbolt county, California. Geology 28(2):111–114

Chandler HW (1985a) A plasticity theory without Drucker's postulate, suitable for granular materails. J Mech Phys Solids 33:215–226

Chandler HW (1990) Homogeneous and localised deformation in granular materials: a mechanistic model. Int J Eng Sci 28(8):719–734

Chandler HW, Sands CM (2007a) An optimisation structure for frictional plasticity. Proc R Soc A Math Phys Eng Sci 463(2084):2005–2020

Chandler HW, Sands CM (2007b) The role of a realistic volume constraint in modelling a two dimensional granular assembly. J Mech Phys Solids 55(7):1341–1356

Chandler HW, Sands CM (2009) A graphical method for producing yield surfaces for soils. Géotechnique 59(8):683–690

Chandler HW, Sands CM (2010) Including friction in the mathematics of classical plasticity. Int J Numer Anal Methods Geomech 34:53–72. doi:10.1002/nag.806

Chupin O, Rechenmacher AL, Abedi S (2011) Finite strain analysis of nonuniform deformation inside shear bands in sands. Int J Numer Anal Methods Geomech 36:1651–1666

Cilona A, Baud P, Tondi E, Agosta F, Vinciguerra S, Rustichelli A, Spiers CJ (2012) Deformation bands in porous carbonate grainstones: field and laboratory observations. J Struct Geol 45(SI):135–155

Collins IF, Houlsby GT (1997) Application of thermomechanical principles to the modelling of geotechnical materials. Proc R Soc Lond Ser A Math Phys Eng Sci 453(1964):1975–2001
Cuss RJ, Rutter EH, Holloway RF (2003) The application of critical state soil mechanics to the mechanical behaviour of porous sandstons. Int J Rock Mech Min Sci 40:847–862
Dan G, Sultan N, Savoye B, Deverchere J, Yelles K (2009) Quantifying the role of sandy-silty sediments in generating slope failures during earthquakes: example from the algerian margin. Int J Earth Sci (Geol Rundsch) 98:769–789
Das A, Buscarnera G (2014) Simulation of localized compaction in high-porosity calcarenite subjected to boundary constraints. Int J Rock Mech Min Sci 71:91–104
DiMaggio FL, Sandler IS (1971) Material models for granular soil. J Eng Mech ASCE 97:939–950
DorMohammadi H, Khoei AR (2008) A three-invariant cap model with isotropic-kinematic hardening rule and associated plasticity for granular materials. Int J Solids Struct 45(2):631–656
Ellis S, Darby D (2005) A modified terzaghi consolidation factor for first-order estimation of overpressure resulting from sedimentation: review and synthesis. Math Geol 37(1):115–123
Fokker PA, Orlic B (2006) Semi-analytic modelling of subsidence. Math Geol 38(5):565–589
Gajo A, Muir Wood D (1999) A kinematic hardening constitutive model for sands: the multiaxial formulation. Int J Numer Anal Methods Geomech 23(9):925–965
Gratchev IB, Sassa K, Osipov VI, Sokolov VN (2006) The liquefactino of clayey soils under cyclic loading. Eng Geol 86:70–84
Han G, Dusseault MB (2005) Sand stress analysis around a producing wellbore with a simplified capillary model. Int J Rock Mech Min Sci 42:1014–1027
Hermanrud C, Venstad JM, Cartwright J, Rennan L, Hermanrud K, Bolåas HMN (2013) Consequences of water level drops for soft sediment deformation and vertical fluid leakage. Math Geosci 45:1–30
Holcomb D, Rudnicki JW, Issen K, Sternlof K (2007) Compaction localization in the earth and the laboratory: state of the research and research directions. Acta Geotech 2(1):1–15
Hunter SC (1976) Mechanics of continuous media, 2nd edn. Ellis Horwood, Chichester
Joer HA, Lanier J, Fahey M (1998) Deformation of granular materials due to rotation of principal axes. Géotechnique 48(5):605–619
Mair K, Abe S (2008) 3d numerical simulations of fault gouge evolution during shear: grain size reduction and strain localization. Earth Planet Sci Lett 274:72–81
Miura N (1979) A consideration on the stress-strain relation of a sand under high pressures. Proc Jpn Soc Civil Eng 282(2):127–130
Miura N, Marata H, Yasufuku N (1984) Stress-strain characteristics of sand in a particle-crushing region. Soils Found 24(1):77–89
Mollema PN, Antonellini MA (1996) Compaction bands: a structural anlogue for anti-mode i cracks in eolian sandstone. Tectonophysics 267:209–228
Paterson SR, Tobisch OT (1993) Pre-lithification structures, deformation mechanisms and fabric ellipsoids in slumped turbidites from the pigeon point formation california. Tectonophysics 222:135–149
Pestana JM, Whittle AJ, Gens A (2002a) Evaluation of a constitutive model for clays and sands: part ii clay behaviour. Int J Numer Anal Methods Geomech 26:1123–1146
Pestana JM, Whittle AJ, Salvati LA (2002b) Evaluation of a constitutive model for clays and sands: part I sand behaviour. Int J Numer Anal Methods Geomech 26:1097–1121
Roscoe KH, Burland JB (1968) On the generalised stress strain behaviour of wet clay. In: Heyman J, Leckie FA (eds) Engineering plasticity. Cambridge University Press, Cambridge, pp 535–609
Sands CM, Chandler HW (2010) Yield surfaces and flow rules for deformation of granular materials with a volume constraint. Comput Geotech 37:701–709
Sands CM, Chandler HW (2011) Simulations of cyclic shearing of sand at low effective stress. Géotechnique 61(11):983–992
Sands CM, Chandler HW (2012) Simulating pressure-induced compaction by grain rearrangement. Géotech Lett 2:187–192
Sands CM, Chandler HW (2014) Methods for incorporating particle rearrangement into compaction using thermodynamic approaches. Contin Mech Thermodyn 26(2):183–192
Sands CM, Chandler HW, Guz IA (2010) Developing elasto-plastic models without establishing any expression for the yield function. Numer Anal Methods Geomech 35:932–946
Sands CM, Brown AR, Chandler HW (2011) The application of principles of soil mechanics to the modelling of pastes. Granul Mater 13:573–584
Tsegaye AB, Benz T (2014) Plastic flow and state-dilatancy for geomaterials. Acta Geotechnica

Vesic AS, Clough GW (1968) Behaviour of granular materials under high stresses. J Soil Mech Found Div ASCE 94(SM3):661–688
Wibberly CJ, Yielding G, Di Toro G (2008) Recent advances in the understanding of fault zone internal structure: a review. Geol Soc Lond Spec Publ 299:5–33
Youd TL (1972) Compaction of sands by repeated shear straining. J Soil Mech Found Div ASCE 98:709–725
Yunus Y, Vincens E, Cambo B (2010) Numerical local analysis of relevant internal variables for constitutive modelling of granular materials. Int J Numer Anal Methods Geomech 34:1101–1123
Zhu C, Arson C (2014) A thermo-mechanical demage model for rock stiffness during anisotropic crack opening and closure. Acta Geomtechnica
Ziegler H (1983) An Introduction to thermomechanics, 2nd edn. North Holland, Amsterdam